# Computational Analysis of Human OGA Structure in Complex with PUGNAc and NAG-Thiazoline Derivatives

Nelson Alberto N. de Alencar,[†] Paulo Robson M. Sousa,[†] José Rogério A. Silva,[†] Jerônimo Lameira,[†,*] Cláudio Nahum Alves,[†] Sergio Martí,[‡] and Vicent Moliner[‡]

[†]Laboratório de Planejamento e Desenvolvimento de Fármacos, Instituto de Ciências Exatas e Naturais, Universidade Federal do Pará, CP 11101, 66075-110, Belém, PA, Brazil

[‡]Departament de Química Física i Analítica, Universitat Jaume I, 12071 Castellón, Spain

**Ⓢ** *Supporting Information*

**ABSTRACT:** The substitution of serine and threonine residues in nucleocytoplasmic proteins with 2-acetamido-2-deoxy-$\beta$-D-glucopyranose (*O*-GlcNAc) residues is an essential post-translational modification found in many multicellular eukaryotes. *O*-glycoprotein 2-acetamino-2-deoxy-$\beta$-D-glucopyranosidase (*O*-GlcNAcase) hydrolyzes *O*-GlcNAc residues from post-translationally modified serine/threonine residues of nucleocytoplasmic protein. *O*-GlcNAc has been implicated in several disease states such as cancer, Alzheimer's disease, and type II diabetes. For this paper, a model of the human *O*-GlcNAcase (hOGA) enzyme based on the X-ray structures of bacterial *Clostridium perfringens* (*Cp*NagJ) and *Bacteroides thetaiotaomicrometer* (*Bt*OGA) homologues has been generated through molecular homology modeling. In addition, molecular docking, molecular dynamics (MD) simulations, and Linear Interaction Energy (LIE) were employed to determine the bind for derivatives of two potent inhibitors: *O*-(2-acetamido-2-deoxy-D-glucopyranosylidene)amino-*N*-phenylcarbamate (PUGNAc) and 1,2-dideoxy-2'-methyl-R-D-glucopyranoso-[2,1-*d*]-Δ2'-thiazoline (NAG-thiazoline), with hOGA. The results show that the binding free energy calculations using the Linear Interaction Energy (LIE) are correlated with inhibition constant values. Therefore, the model of the human *O*-GlcNAcase (hOGA) obtained here may be used as a target for rational design of new inhibitors.
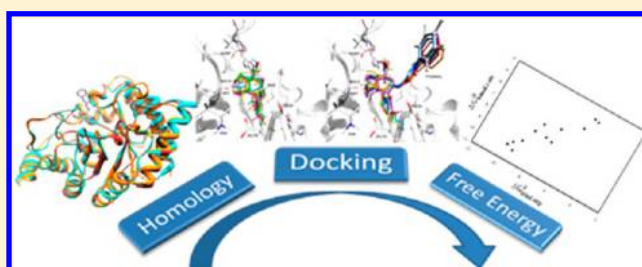
## INTRODUCTION

The post-translational modification of *N-acetylglucosamine* by linking $\beta$-*O*-glucoside of serine and threonine residues of cytoplasmic protein core is called *O*-GlcNAc modification. This modification is commonly found in many proteins with a variety of functions.[1] *O*-GlcNAc is abundant in all multicellular eukaryotes, and its half-life is much shorter than that of the modified polypeptide chain.[2] It has two important characteristic functions: the regulation of phosphorylation and the reversible formation of multimeric complexes with other polypeptides or structures. These associations are often regulated by phosphorylation.[3] *O*-glycoprotein 2-acetamido-2-deoxy-$\beta$-D-glucopyranosidase (*O*-GlcNAcase)[2] is a member of the family of glycoside hydrolases 84 (GH84)[4] that is able to cleave *O*-GlcNAc from post-translationally modified protein serine and threonine residues.[2,3] *O*-GlcNAcase has been used as a target for therapeutic agents[4,5] because disregulation of cellular *O*-GlcNAc levels has been implicated in several diseases including Diabetes II,[6,7] cardiovascular diseases,[8,9] and neurodegenerative processes such as Alzheimer's and Parkinson's disease.[10−14]
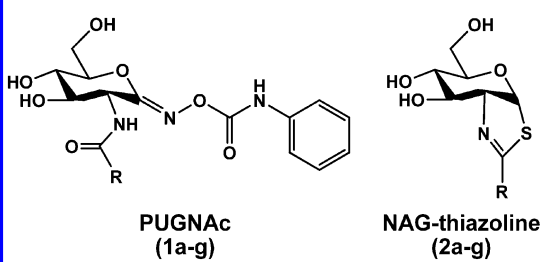
The primary structure of *O*-GlcNAcase has been determined from human brain cells.[15] Human *O*-GlcNAcase (hOGA) is a protein having 916 amino acids with a predicted molecular mass of 103 kDa, which reportedly interacts with several proteins.[12] The N-terminal domain of hOGA contains the catalytic machinery, a TIM barrel structure responsible for a highly conserved amino acids sequence to certain bacterial enzymes from human pathogens and symbionts.[16−18] The hOGA has so far resisted overexpression and purification to the quantities and purity required for structural studies.[15] On the other hand, molecular homology modeling is a well-known computational tool through which it is possible to construct the tertiary structure of a given protein on te basis of knowledge of the primary structure.[19,20] This approach is only possible because the three-dimensional (3D) structure of homologous proteins is conserved during the evolutionary process, especially in the case of the functional residuals, given that conservation of the structure is crucial to the maintenance and development of specific functions.[19,20] The analysis of the CAZY database (http://afmb.cnrs-mrs.fr/cazy) reveals that hOGA is part of GH 84, along with several bacterial enzymes. Among them, we have selected the crystal structure of an enzyme from *Clostridium perfringens* (*Cp*NagJ) and *Bacteroides thetaiotaomicrometer* (*Bt*OGA) as templates for homology modeling study.

**Table 1. PUGNAc and NAG-Thiazoline (NGT) Derivatives with Comparable Inhibition Constants ($K_i$) and $\Delta G^0_{bind,exp}$ Values**

| Inhibitors | R group | PUGNAc | | NAG-thiazoline | |
| --- | --- | --- | --- | --- | --- |
| | | $Ki$ ($\mu$M) | $\Delta G_{bind,exp}$ | $Ki$ ($\mu$M) | $\Delta G_{bind,exp}$ |
| | **a**, -CH$_3$ | 0.046 | -10.07 | 0.07 | -9.82 |
| | **b**, -CH$_2$CH$_3$ | 1.2 | -8.12 | 0.12 | -9.49 |
| | **c**, -(CH$_2$)$_2$CH$_3$ | 2.5 | -7.68 | 0.25 | -9.06 |
| | **d**, -(CH$_2$)$_3$CH$_3$ | 40 | -6.03 | 1.5 | -7.99 |
| | **e**, -(CH$_2$)$_4$CH$_3$ | 220 | -5.02 | 57 | -5.82 |
| | **f**, -CH(CH$_3$)$_2$ | 9 | -6.92 | 1.6 | -7.95 |
| | **g**, -CH$_2$CH(CH$_3$)$_2$ | 190 | -5.10 | 5.7 | -7.19 |



PUGNAc
(1a-g)

NAG-thiazoline
(2a-g)

The crystal structure of *Cp*NagJ in complex with *O*-(2-acetamido-2-deoxy-D-glucopyranosylidene)amino *N*-phenylcarbamate (PUGNAc), a competitive inhibitor of this enzyme in the low nanomolar range, has been shown to have significant sequence homology to the human *O*-GlcNAcase (*Cp*NagJ, 35% sequence identity, 51% sequence similarity).[16] On the other hand, the structure of *O*-GlcNAcase from the human symbiont *Bacteroides thetaiotaomicrometer Bt*OGA[21] also has significant sequence homology to the human *O*-GlcNAcase (*Bt*OGA, 37% sequence identity, 56% sequence similarity), and it was the first crystal structure of an OGA in complex with 1.2 dideoxy-2′-methyl-alpha-D-glucopyranoso[2,1-d]-Delta2′-thiazoline (NAG-thiazoline or NGT). Several PUGNAc and NGT derivatives (Table 1) are characterized as potent inhibitors of hOGA and human Hexosaminidases.[22] These inhibitors have been used to identify the function of *O*-GlcNAc at the cellular level.[6,23,24]

The great interest in therapeutic inhibitors of glycosidases assumes that they have pharmacological activity against viruses, tumors, and metastases, besides the above-mentioned diseases. Because of this, the synthesis and development of new inhibitors is of great value in order to help in treating these diseases and to obtain models for the study of biochemical structure and biological function of glycoproteins.[25] Rao and co-workers suggest that PUGNAc inhibits *O*-GlcNAcase by mimicking the transition state of the *O*-GlcNAcase-catalyzed hydrolysis of N-acetylglucosaminide by virtue of its sp2 anomeric C1, similar to the oxocarbenium ion-like transition state.[16] Whitworth and co-workers claim that NGT is in principle geometrically similar to the oxazoline intermediate and is a transition state analogue for O-GlcNAcase, whereas PUGNAc is a poor transition state analogue.[26,27] In addition, NGT is considered to be more selective than PUGNAc by increasing the methyl group of both; NButGT presents high selectivity (700-fold) over human HexB yet retained good potency for human OGA ($K_i$ = 600 nM at pH7.4).[28,29]

In a previous paper,[30,31] we employed hybrid Quantum Mechanics/Molecular Mechanics (QM/MM)[32] molecular dynamics (MD) simulations to study the details of the *Cp*NagJ-PUGNAc interactions for wild-type and Asp297N, Asp298N, Tyr335F, Asn390A, Asn396A, Asp401A, and Trp490A *Cp*NagJ mutants and to determine electrostatic binding free energy of *Cp*NagJ complexed with both PUGNAc and NGT. We found a strong interaction between Asp401, Asp298, and Asp297 residues and the PUGNAc inhibitor, and

that the electrostatic substrate binding free energy is higher in wild-type, Asn390A, and Trp490A mutants than in the Asp297N, Asp298N, Tyr335PF, Asn396A, and Asp401A ones, in accordance with the experimental results. Furthermore, the NGT-enzyme complex has a binding free energy that is close to the value calculated for the PUGNAc-*Cp*NagJ complex. More recently, we have carried out a complete study of the first step of the catalytic mechanism used by *O*-GlcNAcase involving substrate-assisted catalysis. The free energy profile has shown that formation of the oxazoline intermediate in the O-GlcNAcase catalytic reaction takes place by means of a stepwise mechanism, and PUGNAc would resemble the first transition state of the O-GlcNAcase catalytic reaction path, while NGT would resemble the second transition or intermediate state.[29]

In the work reported here, we employed homology modeling to generate the 3D structure of the catalytic pocket of the human *O*-GlcNAcase (hOGA) protein. Later, we employed docking, molecular dynamics (MD) simulations, and the linear interaction energy (LIE) method to study the details of the protein−ligand interaction for seven derivatives of PUGNAc and seven derivatives of NGT acting as inhibitors of human *O*-GlcNAcase.[26] In order to explain the differences in inhibitory potencies for both hOGA and the *Cp*NagJ enzyme, compounds that inhibit hOGA with comparable inhibition constants ($K_i$) values were selected in the present study (Table 1). These values were obtained with the same experimental protocol, and it is expected that all compounds bind in a similar way in the active site of the hOGA protein.

## ■ COMPUTATIONAL METHODS

**Homology Modeling.** Homology modeling is a well-known tool through which it is possible to construct the tertiary structure of a given protein on the basis of knowledge of the primary structure.[19,33,34] In this report, a first model was obtained using the Swiss-Model Workspace.[33,35,36] Initially, the hOGA primary sequence (NCBI code BAA31654.2) was aligned against the sequence of *Cp*NagJ (35% sequence identity, 51% sequence similarity) with known structure (Protein Data Bank, PDB code: 2CBJ).[16] A second model was obtained using the *Bt*OGA crystal structure (PDB code: 2CHN),[21] as the template also has significant sequence homology to the human *O*-GlcNAcase (*Bt*OGA, 37% sequence identity, 56% sequence similarity). In order to optimize the alignment between the sequence of templates and target, we have carried out a multiple sequence alignment using the

Modeler program, taking into consideration special restriction.[37] The Modeler program was applied to generate 10 satisfactory models for the hOGA. This program uses an automated modeling technique that significantly improves the accuracy of loop predictions in protein structures.[38] The stereochemical quality of the structures was evaluated using Molprobity,[39] while the distribution of residual energy was evaluated with ProSA, version 3.0.[33,34,40] ProSA evaluates the energy of the structure using a distance-based pair potential. Residues with negative ProSA energies confirm the reliability of the model. In addition, Anolea[41] and QMEAN[42] were used to evaluate the model's energy . Finally, the model with the lowest energy and lowest restraint violation was selected for molecular docking study and MD simulations.

**Molecular Docking.** Molecular docking is a key tool in structural molecular biology and computer-assisted drug design.[43] The goal of ligand−protein docking is to predict the predominant binding mode(s) of a ligand with a protein of known three-dimensional structure.[43] In the present study, PUGNAc and NGT derivatives (Table 1) were docked in the hOGA model using AutoDock Vina with a standard set of parameters.[44]

Some preliminary steps were needed to carry out the docking, such as adding polar hydrogens. Once the inhibitors and polar hydrogens were added, the degrees of freedom for the angles of rotation on the bonds were increased to provide greater mobility in the former and thus the possibility of better interaction of the inhibitor on the enzyme. One hundred conformations in ten possibilities of protein−ligand interaction were searched for, in order to obtain good results while considering low computational cost.[44]

The program uses the general conformation dependent scoring function method, which is described as follows

$$c = \sum_{i<j} f_{t_i t_j}(r_{ij})$$

(1)

where, $c$ is the sum $f$ of all pairs of atoms that have a relative motion between them, usually excluding interations of 1−4, atoms that are separated by three covalent bonds in a row. Each atom is assigned as $t_1$ in a symmetrical set of interacting functions $f_{t_i t_j}$, in which we can define the interatomic distance $r_{ij}$. This value can be calculated as the sum of intermolecular and intramolecular contributions as follows

$$c = c_{inter} + c_{intra}$$

(2)

The optimization algorithm described in eq 3 attempts to find the global minimum of $c$ conformations and other low scores to classify them. The predicted binding free energy is calculated from the intermolecular conformation of lowest energy, as shown in eq 1.

$$S_1 = g(c_1 - c_{intra1}) = g(c_{inter1})$$

(3)

where, the function $g$ can be calculated precisely from the increase in the slope of the nonlinear function. On output, other low-energy conformations are also given by the value of 4, but to preserve the ratings, value of $c_{intral}$ is used as the best way to link

$$S_i = g(c_i - c_{intra1})$$

(4)

**Classical MD Simulations.** The computational model for the MD calculations was taken from the model of human hOGA obtained by molecular homology modeling. Once it

became possible to exchange standard p$K_a$ values of the ionizable group with local protein environments,[26] we performed calculation of p$K_a$ values of amino acids within the empirical PROPKA program of Li and co-workers.[45] The results show that most residues were found at their standard protonation state, except Asp175 (p$K_a$ = 5.51) that seems to be protonated at this pH. Interestingly, Asp175 has been proposed as the catalytic acid, protonating the glycosidic bond in the first step of the O-GlcNAcase-catalyzed hydrolysis of N-acetylglucosaminides, while Asp174 polarizes the 2-acetomido substrate group most likely acting as a base in a typical acid/base catalysis.[18] These results are also in agreement with our previous theoretical predictions for CpNagJ.[30]

In this study, the classical MD simulations were carried out using the program Q[46] and the OPLS-AA force field with compatible format for this program. First, the system was solvated with a 25 Å radius simulation sphere of TIP3P water[47] centered on the center of mass of the ligand. Nonbonded interaction energies were calculated up to a 10 Å cutoff, except for the ligand atoms for which no cutoff was used. Beyond the cutoff, long-range electrostatics were treated with the local reaction field (LRF) multiple expansion method.[48,49]

For each of the ligand−protein system simulations, a heating and equilibration procedure was applied before the data collection phase. The equilibration protocol started with 1000 steps of MD using very short time step (0.1 fs) at 1 K temperature, coupled to a strong bath (1 fs bath coupling) with positional restraints on heavy atoms (restrain constant equal at 25 kcal/mol Å[2]). The system was then gradually heated to 300 K during 50 ps, in which the bath coupling was relaxed until the final value of 100 fs, the time step was increased to 1 fs, and the positional restraints were gradually released. Unrestrained MD then followed for 2 ns, with energies collected at regular intervals of 25 fs, according Díaz and co-workers.[48] An advantage of the LIE method is not only its better performance for the calculation of ligand affinities as compared to faster methods like empirical scoring functions, but also that it allows for a physical interpretation of binding contributions. This is important in order to establish structure−activity relationships and assist in further ligand design.[48] Energy averaging was performed on the energetically stable phase of this data collection period (average time for this collection period was 1.1 ns and the shortest collection period was 600 ps). Stability was addressed by comparing the average potential energy values of the first and second halves of the data collection period, which yields the estimated error in calculating the corresponding potential energy.

The MD sampling of the free ligands was done with an equivalent 25 Å TIP3P water sphere. The system was gradually heated with a 50 ps MD trajectory to 300 K, in which the heavy atoms of the ligand were restrained through a 10 kcal/mol Å[2] force constant to their original position. MD followed for at least 2 ns under the same conditions as for the bound state but keeping the center of mass of the ligand restrained to the center of the sphere with a force constant of 10 kcal/mol Å[2]. Trajectory lengths yielding errors in the potential energies not larger than 1 kcal/mol were generally accepted because the computed error in the calculated free energy of binding them is less than 1 kcal/mol.[48,50−54]

**Linear Interaction Energy (LIE).** Molecular dynamics obtained in the previous section in combination with the Linear Interaction Energy method (LIE) were used to calculate the binding affinities.[50,51] This method uses the simulations of the

2777

dx.doi.org/10.1021/ci2006005 | J. Chem. Inf. Model. 2012, 52, 2775−2783

free ligand in solution and the protein−ligand complex to calculate the change in free energy associated with binding to the protein.[50] The difference in interaction energies between them is used to calculate the free energy of binding. The equation used is

$$\Delta G_{\text{LIE}}^{\text{bind}} = \alpha(\langle V_{1-s}^{\text{vdW}}\rangle_{\text{bound}} - \langle V_{1-s}^{\text{vdW}}\rangle_{\text{free}})$$
$$+ \beta(\langle V_{1-s}^{\text{el}}\rangle_{\text{bound}} - \langle V_{1-s}^{\text{el}}\rangle_{\text{free}}) \qquad (5)$$

where the $\alpha$ parameter is the empirically derived nonpolar scaling factor, and $\beta$ is the scaling factor of the polar contribution dependent on the chemical nature of the ligand. The term $\langle V_{1-s}^{\text{vdW}}\rangle$ represents the average of the ligand-surrounding van der Waals (water plus protein in the "bound" case and only water in the "free" term subscript). The term $\langle V_{1-s}^{\text{el}}\rangle$ represents the average for electrostatic interaction energies from the simulations of bound and free ligand.[50,51] In these systems the coefficient $\alpha$ has been empirically set to a value of 0.181, while for the $\beta$ coefficient the value adopted was 0.33 for ligands that contained two or more hydroxyl groups.[48,50−54]

Finally, binding free energy estimates were compared to experimentally measured $K_i$ values, which were converted into experimental free energy values using the equation

$$\Delta G_{\text{bind,exp}}^0 = -RT\ln(1/K_i)$$

## RESULTS AND DISCUSSION

**Homology Modeling of the hOGA Protein.** A region corresponding to amino acids 67−442 in the amino terminus was hypothesized to contain the catalytic glycoside hydrolase domain of O-GlcNAcase. The N-terminal domain has been proposed as responsible for glycoside hydrolase activity.[4] The hOGA has so far resisted overexpression and purification to quantities and purity required for structural studies.[16] To gain insight into the structure and function of hOGA, we have modeled the 3D structure of the hOGA N-terminus by molecular homology modeling, as explained in the Homology Modeling section. Figure 1 shows the superposition of the hOGA N-terminus with CpNagJ and BtOGA 3D structures, while Figure 2 shows the multiple alignment sequence of CpNagJ and BtOGA with the hOGA N-terminus. For both models, the hOGA N-terminus presented significant homology,



**Figure 1.** Superposition of the hOGA N-terminus with CpNagJ and BtOGA 3D structures.

and all important residues in the catalytic site were conserved. The stereochemical quality of the model from homology modeling was checked with the Molprobity program[39] (Figure 3). The majority of the residues of the model and template were found to occupy the most favored regions of the Ramachandran plot, and other residues occupied the additional allowed regions.

These plots represent the distribution of the $\Phi$ and $\psi$ angles in each residual of the amino acid. In the model, 92.58% of the residues were presented in the favored regions (95.63% were found for template). Furthermore, the quality of the structure derived from homology modeling was validated by calculating the ProSA Z-score (evaluating overall model quality by C$\alpha$ positions).[33,34,40] The Z-score of the model was −7.20. The atomic empirical mean force potential ANOLEA[41] was used to assess packing quality of the model. The program performs energy calculations on a protein chain, evaluating the non-local environment of each heavy atom in the molecule (Figure S1, Support information).

The catalytic pocket of the hOGA N-terminus model presents a classical TIM barrel structure $(\beta/\alpha)_8$ with the seventh helix replaced by a turn. It thus comprises seven $\alpha$-helices ($\alpha$1, $\alpha$2, $\alpha$3, $\alpha$4, $\alpha$5, $\alpha$6, $\alpha$8) and eight $\beta$-sheets ($\beta$1, $\beta$2, $\beta$3, $\beta$4, $\beta$5, $\beta$6, $\beta$7, $\beta$8) (Figure 4), showing that most of the secondary structure elements in the N-terminus domains are conserved, as described for other homologous crystallographic structures deposited in the PDB. Asp174 and Asp175, located respectively between $\alpha$4 and $\beta$4, and Asp285, located between the turn that replaces $\alpha$7 and $\beta$7, occupy equivalent positions to those of the catalytic residues (Asp297/Asp298/Asp401) in CpNagJ and (Asp242/Asp243/Asp344) in BtOGA (Figure 4).

The numbers of hydrophobic interactions, ionic interactions, aromatic−aromatic interactions, and cation $\pi$ interactions were calculated using a Protein Interactions Calculator Server.[33,55] The results of these calculations are summarized in Figure S2 of the Support information. There is not much difference between CpNagJ, BtOGA, and hOGA. The CpNagJ is more hydrophobic because of presenting a higher number of amino acid residues with apolar character; however, the number of hydrophobic interactions between BtOGA and hOGA is very similar. The ionic interactions present in the active site of the three enzymes show high similarity; two would be Asp174 and Asp175 in hOGA that have strong ionic interactions with Lys36 with 3.2 Å. Additionally, we found very many amino acids completely conserved into proteins studied here, indicating that the comparative modeling of proteins is an interesting tool for elucidation of the 3D structure O-GlcNAcase human.

**Molecular Docking of PUGNAc and NGT Derivatives in hOGA.** In order to investigate how the PUGNAc and NGT derivatives bind the active site of hOGA, we docked PUGNAc and NGT derivatives (Table 1) into the modeled active site of hOGA. Five poses of each inhibitor were computed in the active site during the docking process. We chose the best position for each one by ranking the affinity energy (EA); see Table S1 of the Supporting Information. Figure 5a and b show the positions for PUGNAc and NGT derivatives in the active site of the hOGA, respectively. As observed in Figure 5c and d, the best docked position of PUGNAc and NGT is close to the experimental data[16,21] complex with rmsd of 0.21 and 0.26 Å, respectively. The results of affinity energy (EA) for the best ranking positions of PUGNAc and NGT derivatives reveal a modest correlation with $\Delta G_{\text{bind,exp}}^0$ values for the PUGNAc and NGT derivatives ($R^2 = 0.53$ and 0.57 for hOGA, respectively).
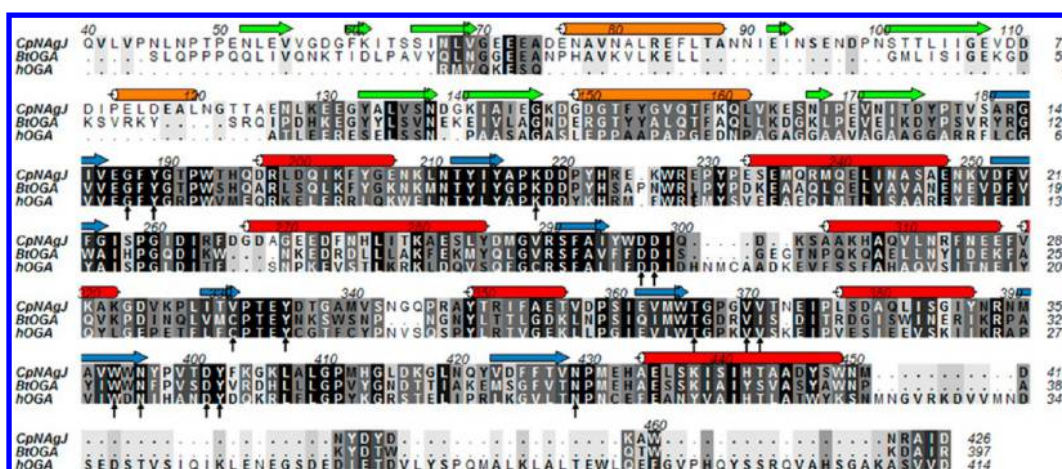
2778

dx.doi.org/10.1021/ci2006005 | J. Chem. Inf. Model. 2012, 52, 2775−2783

**Figure 2.** Multiple alignment sequence of *Cp*NagJ and *Bt*OGA with the hOGA N-terminus.
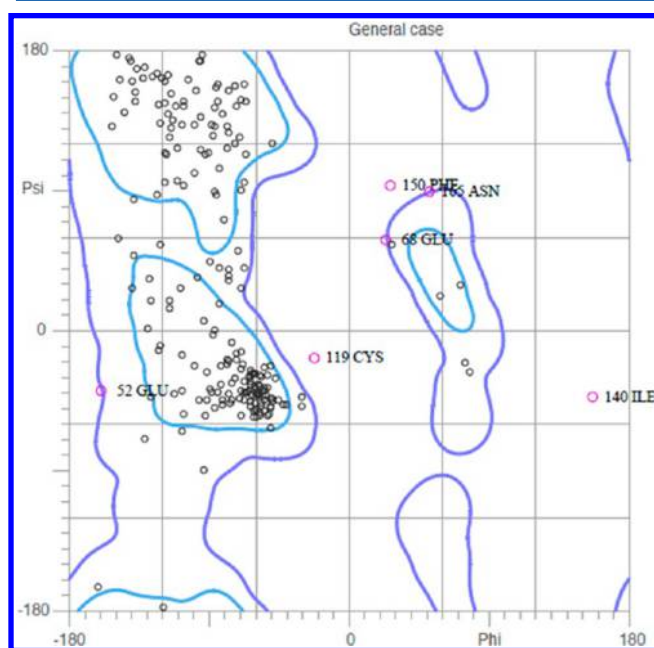


**Figure 3.** Stereochemical quality of the model from homology modeling with the Molprobity program.

A recent study has suggested that within the hOGA family, 84 enzymes Asp174 and Asp175 are the key catalytic residues.[18] These residues correspond to Asp297 and Asp298 within *Cp*NagJ[16] and occupy equivalent positions to those of *Bt*OGA,[20] which are found in the N-terminal domain. After the molecular docking, the Asp175 is within hydrogen bonding distance of oxime nitrogen for the PUGNAc analogs and Asp174 is within hydrogen bonding distance of the acetamido group, which is in agreement with experimental data[15] (Figure 5 and Table 2). On the other hand, the Asp174 is positioned to form a hydrogen bond with the nitrogen of the thiazoline ring of the NGT analogs. Other important residues presenting an interaction with these inhibitors are Asn280, Asn313, and Tyr219. Asp285 presents favorable interactions with O4 and O6 hydroxyl oxygen atoms of the inhibitor. Asn313 also presents interaction with O sugar hydroxyls. The distance between OH of Tyr219 and oxime nitrogen of PUGNAc is 2.26 Å, 2.29 Å, respectively. A recent study has suggested that Tyr219 would be positioned to stabilize any partial negative charge that develops at the glycosidic oxygen in such a

transition state, consistent with the requirement of this residue for catalysis.[16] These results are in agreement with experimental measurements by Rao and co-workers for *Cp*NagJ[16] and Dennis et al. for *Bt*OGA.[21] In general, the complex obtained by homology modeling and docking is close to the crystallographic structures. Table 2 summarizes the key distances obtained from molecular docking for PUGNAc-hOGA and NGT-hOGA complexes.

**MD Simulations and LIE.** As explained in the Computational Methods section, MD simulations of 2 ns were carried out for the hOGA model in complex with PUGNAc and NGT derivatives. Furthermore, 2 ns MD simulations in water were performed for each compound. Therefore, a total of 56 ns MD simulations were performed. During the MD simulation, the rmsd drift of the $C\alpha$ atoms in the initial hOGA model was determined (Figure S3, Supporting Information). When we examine the deviation of the protein during MD simulation, it is clear that the hOGA model has considerable stability. In addition, according to the ANOLEA graphic that performs energy calculations at the atomic level in protein structures, the molecular dynamics considerably improved the model, decreasing the energy. The hOGA model before the molecular dynamic has unfavorable energy in different regions in the protein (Figure S1, Supporting Information).

The mean distances computed during 2 ns of MD for PUGNAc and NGT derivatives are depicted in Table 2. These distances can be compared with previous experimental data for PUGNAc-*Cp*NagJ and NGT-*Bt*OGA complexes.[26] The docking results and mean distances obtained from MD show that Asp174 is positioned to form a hydrogen bonding with amide nitrogen stabilizing the charges of the pyranose ring for both inhibitors, while Asp175 engages only with PUGNAc through hydrogen bonding with exocyclic oxime nitrogen, assisting in the interaction with the general acid/base catalytic group.[21,26] In general, the Lys98, Asp175 (1a-hOGA complex), Asp174 (2a-hOGA complex), and Asp285 residues that form hydrogen bonds to both inhibitors, maintain their stability during the molecular dynamics (Table 2), which is in accordance with experimental data.[16,21] On the other hand, some averaged distances for the inhibitor-protein computed during MD simulations present considerable deviation (Table 2) from experimental data.[16,21] Averaged distances between the inhibitor and Gly67, Asn280, and Asn313 residues are not in agreement with experimental data. As observed in Table 2, the distance between O of Gly67 and O6 of inhibitor is 2.56, 2.02,

2779

dx.doi.org/10.1021/ci2006005 | *J. Chem. Inf. Model.* 2012, 52, 2775–2783
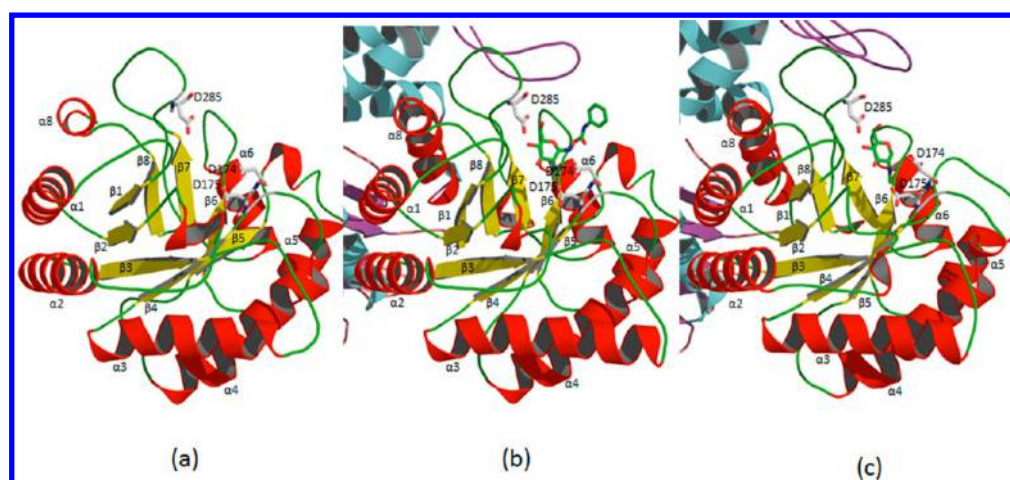
**Figure 4.** Comparison of the catalytic pocket of the (a) hOGA N-terminus, (b) *Cp*NagJ, and (c) *Bt*OGA. The structures are shown in a ribbon representation with red helices and blue strands for the TIM barrel (labeled with $(\beta/\alpha)_8$). The catalytic residues Asp174/Asp175/Asp285 are shown in white for the hOGA structure, while the equivalent aspartates are also shown for *Cp*NagJ and *Bt*OGA. The PUGNAc and NGT inhibitors are shown in green on the respective PDB structures.
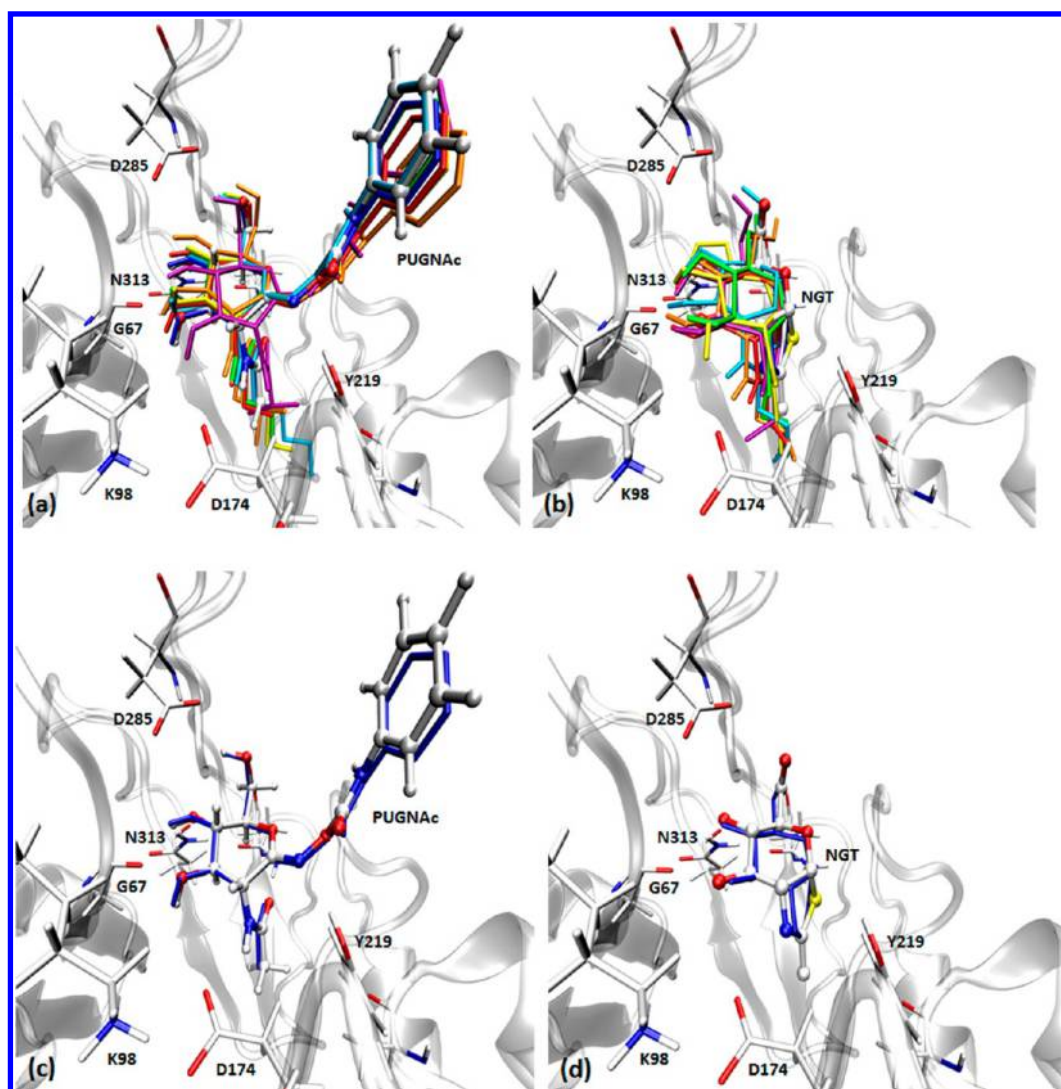


**Figure 5.** (a) and (b) The best docked position of PUGNAc and NGT derivatives in the active site of the hOGA, respectively. (c) and (d) Superposition of the best docked position of **1a** and **2a** compound with the experimental data (*Cp*NagJ and *Bt*OGA).

2780

dx.doi.org/10.1021/ci2006005 | *J. Chem. Inf. Model.* 2012, 52, 2775−2783

**Table 2. Summarizes Key Distances Obtained from Molecular Docking, Mean Distances Computed during 2 ns of MD for PUGNAc (1a) and NGT (2a) in Complex with hOGA and Experimental Data Values**

| hOGA | I − G67 | I − K98 | I − D174 | I − D175 | I − N280 | I − D285 | I − D285 | I − N313 |
|---|---|---|---|---|---|---|---|---|
| | O6 − O | O6 − NZ | N4 − OD2 | N15 − OD1 | O3 − ND2 | O12 − OD1 | O8 − OD2 | O8 − ND2 |
| 1a-*Cp*NagJ[a] | 2.56 | 2.96 | 2.77 | 2.88 | 2.81 | 2.43 | 2.45 | 3.11 |
| 1a-hOGA (Docked) | 2.02 | 2.51 | 2.97 | 2.95 | 2.99 | 2.90 | 2.94 | 3.13 |
| 1a-hOGA (LIE) | 3.14 (0.34) | 2.93 (0.55) | 2.85 (0.14) | 2.97 (0.12) | 4.95 (0.99) | 2.67 (0.11) | 2.65 (0.10) | 3.03 (0.22) |
| | O6 − O | O6 − NZ | N4 − OD2 | − | S2 − ND2 | O12 − OD1 | O8 − OD2 | O8 − ND2 |
| 2a-*Bt*OGA[a] | 2.64 | 2.96 | 2.93 | − | 3.27 | 2.83 | 2.60 | 3.05 |
| 2a-hOGA (Docked) | 3.28 | 3.05 | 2.79 | − | 2.94 | 2.96 | 2.77 | 3.20 |
| 2a-hOGA (LIE) | 4.50 (0.84) | 3.26 (0.39) | 2.66 (0.12) | − | 3.63 (0.28) | 2.65 (0.11) | 2.73 (0.13) | 5.33 (1.01) |

[a]Experimental values obtained from refs 16 and 21.

**Table 3. Average Ligand-Surrounding Energies (kcal/mol) Computed during the Last 500 ps of MD for the Inhibitors Studied**

| Inhibitors | $\langle V^{vdW}_{1-s}\rangle_{bound}$ | $\langle V^{vdW}_{1-s}\rangle_{free}$ | $\langle V^{el}_{1-s}\rangle_{bound}$ | $\langle V^{el}_{1-s}\rangle_{free}$ | $\Delta G^0_{bind,calc}$ | $\Delta G^0_{bind,exp}$ |
|---|---|---|---|---|---|---|
| 1a | −34.22 | −23.13 | −107.82 | −85.72 | −9.30 | −10.07 |
| 1b | −39.24 | −24.79 | −104.31 | −90.22 | −7.26 | −8.12 |
| 1c | −45.07 | −26.52 | −101.20 | −92.31 | −6.30 | −7.86 |
| 1d | −47.65 | −28.25 | −99.61 | −92.67 | −5.80 | −6.03 |
| 1e | −50.25 | −29.88 | −98.33 | −92.92 | −5.47 | −5.02 |
| 1f | −40.70 | −26.30 | −100.14 | −86.41 | −7.14 | −6.92 |
| 1g | −46.56 | −27.98 | −91.84 | −86.38 | −5.16 | −5.10 |
| 2a | −23.85 | −14.15 | −64.74 | −40.36 | −9.80 | −9.82 |
| 2b | −24.50 | −15.30 | −71.43 | −47.58 | −9.53 | −9.49 |
| 2c | −30.41 | −17.28 | −60.53 | −40.32 | −9.04 | −9.06 |
| 2d | −34.32 | −19.35 | −56.76 | −41.58 | −7.72 | −7.99 |
| 2e | −34.69 | −20.03 | −61.48 | −43.97 | −8.43 | −5.82 |
| 2g | −29.18 | −16.81 | −64.48 | −45.25 | −8.60 | −7.95 |
| 2f | −33.54 | −18.16 | −59.26 | −42.57 | −8.29 | −7.19 |

and 3.14 for X-ray crystallographic structure, PUGNAc-protein complex obtained from molecular docking, and the mean distances computed during 2 ns of MD for the PUGNAc-protein complex, respectively. Meanwhile, this distance obtained by X-ray crystallographic, molecular docking, and MD simulations correspond to 2.64, 3.28, and 4.45, for NGT-protein complex, respectively (Table 2). In addition, the distance between ND2 of Asn280 and O3 of 1a inhibitor correspond to 2.56, 2.02, and 3.14 for X-ray crystallographic structure, PUGNAc-protein complex obtained from molecular docking, and the mean distances computed during 2 ns of MD, respectively. Lastly, the distance between ND2 of Asn313 and O8 of 2a inhibitor is 3.05, 3.20, and 5.33 for X-ray crystallographic structure and theoretical structures obtained from molecular docking and MD simulations, respectively. As molecular docking was performed using the model obtained from molecular homology modeling, the distance deviation (Table 2) from experimental data may be explained by structural differences between 3D structures of the hOGA N-terminus, *Cp*NagJ, and *Bt*OGA. Despite this fact, PUGNAc (1a) and NAG-thiazoline (2a) patterns of interaction within the hOGA model active site are very similar.

Regarding the series of PUGNAc and NAG-thiazoline derivatives, the structural changes within compounds studied here are a small increase in the volume of alkyl group of the N-acyl moiety, which leads to a rise in $K_i$ values when assayed against hOGA. However, the bind change observed for these inhibitors is more correlated with C log P than with the molecular volume of inhibitors (Table S2, Supporting Information). In order to contribute to designing compounds with more interesting inhibitory activity on the basis of their three-dimensional structure, we have determined the absolute binding using LIE as described below.

The absolute binding calculated for the NAG-thiazoline (2a) inhibitor using LIE (−9.80 kcal/mol) is in agreement with the experimental values ($\Delta G^0_{bind,exp}$ = −9.82 kcal/mol). On the other hand, the absolute binding calculated for the PUGNAc (1a) inhibitor using the same methodology (−9.30 kcal/mol) reproduces the experimental affinities ($\Delta G^0_{bind,exp}$ = −10.07 kcal/mol) with an error of 0.77 kcal/mol. In general, calculations of bind affinities from MD trajectories through the LIE method are in excellent agreement with experimental data[26] (Table 3). From comparison between the theoretical predictions and the experimentally measured kinetic data for all complexes, it seems that the free energy calculations are reliable for practically all derivatives in complex with the hOGA model. The coefficient of determination obtained for the linear fit of predicted values versus the observed contributions was modest ($r^2$ = 0.67). The reason is the absolute binding calculated for 1c and 2e compounds using LIE, which presents a considerable deviation (1.56 and 2.61 kcal/mol, respectively) when compared with experimental values. When these compounds are excluded from the model the coefficient of determination observed is 0.89 (the linear correlation is depicted in Figure 6). These results suggest that the standard parametrization of LIE is a robust method that reproduces the experimental affinities.

■ CONCLUSIONS

In this report, molecular docking, molecular homology modeling, MD simulations, and LIE were employed to provide
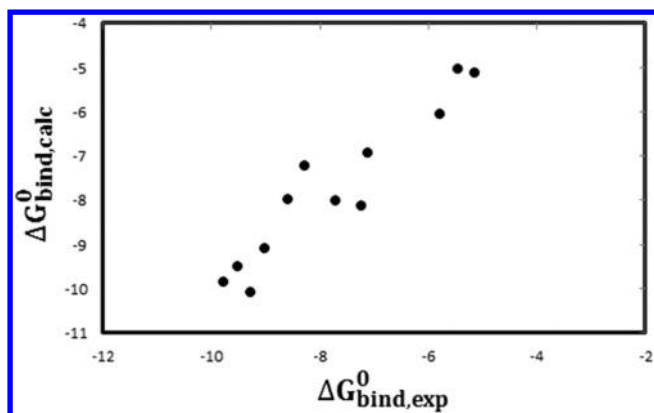
**Figure 6.** Linear correlation between $\Delta G^0_{bind,calc}$ and $\Delta G^0_{bind,exp}$ (kcal/mol) excluding **1c** and **2e** compounds of the model.

insights into the activity of PUGNAc and NGT derivatives against human *O*-GlcNAcase. The model of the hOGA N-terminal domain obtained by homology modeling suggests that the active sites of *Cp*NagJ, *Bt*OGA, and hOGA are similar, which is in agreement with the similar position of PUGNAc and NGT in both in these respective enzymes. The analysis of individual interactions between the inhibitor and the amino acids of the enzyme active site, averaged alongside the MD simulation, reveals how the influence of Asp285, Asp174, Asp175, and Tyr219 in the hOGA seems to be crucial, with the interactions established between the inhibitor and these residues being especially important. Finally, comparing the theoretical predictions on both hOGA-PUGNAc and hOGA-NGT complexes with the experimentally measured kinetic data, $K_i$, it seems that the bind affinity obtained through LIE calculations is in excellent agreement with experimental data. Thus, we conclude that the model of hOGA obtained by homology modeling seems to be a good candidate for studying the active site of this enzyme in order to design new more potent and specific inhibitors.

## ASSOCIATED CONTENT

### Supporting Information
Figures S1–S3 and Tables S1 and S2. Figure S1 shows ANOLEA plot before and after dynamic for the model; Figure S2 shows numbers of hydrophobic interactions, ionic interactions, aromatic–aromatic interactions, and cation-$\pi$ interactions; Figure S3 shows the rmsd drift of the C$\alpha$ atoms computed during the first 1.5 ns of MD for the NGT derivatives. Affinity energy (EA) for the best ranking positions of PUGNAc and NGT are depicted in Table S1. Table S2 shows molecular volume and ClogP of inhibitors studied.

This information is available free of charge via the Internet at http://pubs.acs.org.

## AUTHOR INFORMATION

### Corresponding Author
*E-mail: lameira@ufpa.br. Phone: (+55) 91-32018235. Fax: (+55) 91-32017633.

### Notes
The authors declare no competing financial interest.

## ACKNOWLEDGMENTS

## REFERENCES

(1) Hart, G. W.; Housley, M. P.; Slawson, C. Cycling of O-linked beta-N-acetylglucosamine on nucleocytoplasmic proteins. *Nature* **2007**, *446*, 1017−1022.

(2) Wells, L.; Vosseller, K.; Hart, G. W. Glycosylation of nucleocytoplasmic proteins: Signal transduction and O-GlcNAc. *Science* **2001**, *291*, 2376−2378.

(3) Dias, W. B.; Hart, G. W. O-GlcNAc modification in diabetes and Alzheimer's disease. *Mol. Biosyst.* **2007**, *3*, 766−772.

(4) Hanover, J. A. Glycan-dependent signaling: O-linked N-acetylglucosamine. *Faseb J.* **2001**, *15*, 1865−1876.

(5) Arnold, C. S.; Johnson, G. V. W.; Cole, R. N.; Dong, D. L. Y.; Lee, M.; Hart, G. W. The microtubule-associated protein tau is extensively modified with O-linked N-acetylglucosamine. *J. Biol. Chem.* **1996**, *271*, 28741−28744.

(6) Vosseller, K.; Wells, L.; Lane, M. D.; Hart, G. W. Elevated nucleocytoplasmic glycosylation by O-GlcNAc results in insulin resistance associated with defects in Akt activation in 3T3-L1 adipocytes. *Proc. Natl. Acad. Sci. U.S.A.* **2002**, *99*, 5313−5318.

(7) McClain, D. A.; Lubas, W. A.; Cooksey, R. C.; Hazel, M.; Parker, G. J.; Love, D. C.; Hanover, J. A. Altered glycan-dependent signaling induces insulin resistance and hyperleptinemia. *Proc. Natl. Acad. Sci. U.S.A.* **2002**, *99*, 10695−10699.

(8) Jones, S. P.; Zachara, N. E.; Ngoh, G. A.; Hill, B. G.; Teshima, Y.; Bhatnagar, A.; Hart, G. W.; Marban, E. Cardioprotection by N-acetylglucosamine linkage to cellular proteins. *Circulation* **2008**, *117*, 1172−1182.

(9) Downey, J. M.; Cohen, M. V. O-linked beta-N-acetylglucosamine: A new piece of the cardioprotection puzzle? *Circ. Res.* **2009**, *104*, 7−8.

(10) Griffith, L. S.; Schmitz, B. O-linked n-acetylglucosamine is up-regulated in alzheimer brains. *Biochem. Biophys. Res. Commun.* **1995**, *213*, 424−431.

(11) Yao, P. J.; Coleman, P. D. Reduction of O-linked N-acetylglucosamine-modified assembly protein-3 in Alzheimer's disease. *J. Neurosci.* **1998**, *18*, 2399−2411.

(12) Liu, F.; Iqbal, K.; Grundke-Iqbal, I.; Hart, G. W.; Gong, C. X. O-GlcNAcylation regulates phosphorylation of tau: A mechanism involved in Alzheimer's disease. *Proc. Natl. Acad. Sci. U.S.A.* **2004**, *101*, 10804−10809.

(13) Skorobogatko, Y. V.; Deuso, J.; Adolf-Bryfogle, J.; Nowak, M. G.; Gong, Y.; Lippa, C. F.; Vosseller, K. Human Alzheimer's disease synaptic O-GlcNAc site mapping and iTRAQ expression proteomics with ion trap mass spectrometry. *Amino acids* **2011**, *40*, 765−779.

(14) Yuzwa, S. A.; Shan, X.; Macauley, M. S.; Clark, T.; Skorobogatko, Y.; Vosseller, K.; Vocadlo, D. J. Increasing O-GlcNAc slows neurodegeneration and stabilizes tau against aggregation. *Nat. Chem. Biol.* **2012**, *8*, 393−399.

(15) Ishikawa, K.; Nagase, T.; Suyama, M.; Miyajima, N.; Tanaka, A.; Kotani, H.; Nomura, N.; Ohara, O. Prediction of the coding sequences of unidentified human genes. X. The complete sequences of 100 new cDNA clones from brain which can code for large proteins in vitro. *DNA Res.* **1998**, *5*, 169−176.

(16) Rao, F. V.; Dorfmueller, H. C.; Villa, F.; Allwood, M.; Eggleston, I. M.; van Aalten, D. M. F. Structural insights into the mechanism and inhibition of eukaryotic O-GlcNAc hydrolysis. *Embo J.* **2006**, *25*, 1569−1578.

(17) Gao, Y.; Wells, L.; Comer, F. I.; Parker, G. J.; Hart, G. W. Dynamic O-glycosylation of nuclear and cytosolic proteins - Cloning and characterization of a neutral, cytosolic beta-N-acetylglucosamini-dase from human brain. *J. Biol. Chem.* **2001**, *276*, 9838−9845.

(18) Cetinbas, N.; Macauley, M. S.; Stubbs, K. A.; Drapala, R.; Vocadlo, D. J. Identification of Asp(174) and Asp(175) as the key catalytic residues of human O-GlcNAcase by functional analysis of site-directed mutants. *Biochemistry* **2006**, *45*, 3835−3844.

(19) Marti-Renom, M. A.; Stuart, A. C.; Fiser, A.; Sanchez, R.; Melo, F.; Sali, A. Comparative protein structure modeling of genes and genomes. *Annu. Rev. Biophys. Biomol. Struct.* **2000**, *29*, 291−325.

(20) Höltje, H. D.; Sippl, W.; Rognan, D.; Folkers, G. *Molecular Modeling: Basic Principles and Applications*,3rd ed.; Kukol, A., Ed.; Wiley-VCH: Weinhein, Germany, 2008; pp 365−382.

(21) Dennis, R. J.; Taylor, E. J.; Macauley, M. S.; Stubbs, K. A.; Turkenburg, J. P.; Hart, S. J.; Black, G. N.; Vocadlo, D. J.; Davies, G. J. Structure and mechanism of a bacterial beta-glucosaminidase having O-GlcNAcase activity. *Nat. Struct. Mol. Biol.* **2006**, *13*, 365−371.

(22) Macauley, M. S.; Whitworth, G. E.; Debowski, A. W.; Chin, D.; Vocadlo, D. J. O-GlcNAcase uses substrate-assisted catalysis: Kinetic analysis and development of highly selective mechanism-inspired inhibitors. *J. Biol. Chem.* **2005**, *280*, 25313−25322.

(23) Gandy, J. C.; Rountree, A. E.; Bijur, G. N. Akt1 is dynamically modified with O-GlcNAc following treatments with PUGNAc and insulin-like growth factor-1. *FEBS Lett.* **2006**, *580*, 3051−3058.

(24) Laczy, B.; Marsh, S. A.; Brocks, C. A.; Wittmann, I.; Chatham, J. C. Inhibition of O-GlcNAcase in perfused rat hearts by NAG-thiazolines at the time of reperfusion is cardioprotective in an O-GlcNAc-dependent manner. *Am. J. Physiol. Heart. Circ. Physiol.* **2010**, *299*, 1715−1727.

(25) Melo, E. B. d.; Carvalho, I. a e b-glucosidases como alvos moleculares para desenvolvimento de fármacos. *Química Nova* **2006**, *29*, 840−843.

(26) Whitworth, G. E.; Macauley, M. S.; Stubbs, K. A.; Dennis, R. J.; Taylor, E. J.; Davies, G. J.; Greig, I. R.; Vocadlo, D. J. Analysis of PUGNAc and NAG-thiazoline as transition state analogues for human O-GlcNAcase: Mechanistic and structural insights into inhibitor selectivity and transition state poise. *J. Am. Chem. Soc.* **2007**, *129*, 635−644.

(27) Yuzwa, S. A.; Macauley, M. S.; Heinonen, J. E.; Shan, X.; Dennis, R. J.; He, Y.; Whitworth, G. E.; Stubbs, K. A.; McEachern, E. J.; Davies, G. J.; Vocadlo, D. J. A potent mechanism-inspired O-GlcNAcase inhibitor that blocks phosphorylation of tau in vivo. *Nat. chem. biol.* **2008**, *4*, 483−490.

(28) Macauley, M. S.; Vocadlo, D. J. Increasing O-GlcNAc levels: An overview of small-molecule inhibitors of O-GlcNAcase. *Biochim. Biophys. Acta* **2010**, *1800*, 107−121.

(29) Lameira, J. n.; Alves, C. u. N.; Tuñón, I. a.; Martí, S.; Moliner, V. Enzyme molecular mechanism as a starting point to design new inhibitors: A theoretical study of O-GlcNAcase. *J. Phys. Chem. B* **2011**, *115*, 6764−6775.

(30) Lameira, J.; Alves, C. N.; Moliner, V.; Marti, S.; Kanaan, N.; Tunon, I. A Quantum mechanics/molecular mechanics study of the protein-ligand interaction of two potent inhibitors of human O-GlcNAcase: PUGNAc and NAG-thiazoline. *J. Phys. Chem. B* **2008**, *112*, 14260−14266.

(31) Lameira, J.; Alves, C. N.; Moliner, V.; Marti, S.; Castillo, R.; Tunon, I. Quantum mechanical/molecular mechanical molecular dynamics simulation of wild-type and seven mutants of CpNagJ in complex with PUGNAc. *J. Phys. Chem. B* **2010**, *114*, 7029−7036.

(32) Warshel, A.; Levitt, M. Theoretical studies of enzymic reactions: Dielectric, electrostatic and steric stabilization of carbonium-ion in reaction of lysozyme. *J. Mol. Biol.* **1976**, *103*, 227−249.

(33) Silva, J. R. A.; Lameira, J.; Santana, P. P. B.; Silva, A.; Schneider, M. P. C.; Alves, C. N. Homology modeling and molecular dynamics simulation of an alpha methyl coenzyme M reductase from methanogenic archea. *Int. J. Quantum Chem.* **2010**, *110*, 2067−2075.

(34) Lima, A. H.; Souza, P. R. M.; Alencar, N.; Lameira, J.; Govender, T.; Kruger, H. G.; Maguire, G. E. M.; Alves, C. N. Molecular modeling of *T. rangeli*, *T. brucei gambiense*, and *T. evansi sialidases* in complex with the DANA inhibitor. *Chem. Biol. Drug Des.* **2012**, *80*, 114−120.

(35) Arnold, K.; Bordoli, L.; Kopp, J.; Schwede, T. The SWISS-MODEL workspace: A web-based environment for protein structure homology modelling. *Bioinformatics* **2006**, *22*, 195−201.

(36) Schwede, T.; Kopp, J.; Guex, N.; Peitsch, M. C. SWISS-MODEL: An automated protein homology-modeling server. *Nucleic Acids Res.* **2003**, *31*, 3381−3385.

(37) Sali, A.; Blundell, T. L. Comparative protein modelling by satisfaction of spatial restraints. *J. Mol. Biol.* **1993**, *234*, 779−815.

(38) Fiser, A.; Do, R. K.; Sali, A. Modeling of loops in protein structures. *Protein Sci.* **2000**, *9*, 1753−1773.

(39) Davis, I. W.; Murray, L. W.; Richardson, J. S.; Richardson, D. C. MOLPROBITY: Structure validation and all-atom contact analysis for nucleic acids and their complexes. *Nucleic Acids Res.* **2004**, *32*, 615−619.

(40) Wiederstein, M.; Sippl, M. J. ProSA-web: Interactive web service for the recognition of errors in three-dimensional structures of proteins. *Nucleic Acids Res.* **2007**, *35*, 407−410.

(41) Melo, F.; Feytmans, E. Assessing protein structures with a non-local atomic interaction energy. *J. Mol. Biol.* **1998**, *277*, 1141−1152.

(42) Benkert, P.; Tosatto, S. C. E.; Schomburg, D. QMEAN: A comprehensive scoring function for model quality assessment. *Proteins* **2008**, *71*, 261−277.

(43) Morris, G. M.; Lim-Wilby, M. Methods in Molecular Docking. In *Molecular Modeling of Proteins*; Kukol, A., Ed.; Humana Press: Totowa, NJ, 2008; pp 365−382.

(44) Trott, O.; Olson, A. J. AutoDock Vina: Improving the speed and accuracy of docking with a new scoring function, efficient optimization, and multithreading. *J. Comput. Chem.* **2010**, *31*, 455−461.

(45) Li, H.; Robertson, A. D.; Jensen, J. H. Very fast empirical prediction and rationalization of protein pKa values. *Proteins: Struct., Funct., Bioinf.* **2005**, *61*, 704−721.

(46) Marelius, J.; Kolmodin, K.; Feierberg, I.; Åqvist, J. Q: A molecular dynamics program for free energy calculations and empirical valence bond simulations in biomolecular systems. *J. Mol. Graphics Modell.* **1998**, *16*, 213−225.

(47) Jorgensen, W. L.; Chandrasekhar, J.; Madura, J. D.; Impey, R. W.; Klein, M. L. Comparison of simple potential functions for simulating liquid water. *J. Chem. Phys.* **1983**, *79*, 926−935.

(48) Diaz, L.; Bujons, J.; Delgado, A.; Gutierrez-de-Teran, H.; Aqvist, J. Computational prediction of structure-activity relationships for the binding of aminocyclitols to beta-glucocerebrosidase. *J. Chem. Inf. Model.* **2011**, *51*, 601−611.

(49) Lee, F. S.; Warshel, A. A local reaction field method for fast evaluation of long-range electrostatic interactions in molecular simulations. *J. Chem. Phys.* **1992**, *97*, 3100−3107.

(50) Åqvist, J.; Medina, C.; Samuelsson, J.-E. A new method for predicting binding affinity in computer-aided drug design. *Protein Eng.* **1994**, *7*, 385−391.

(51) Gutierrez-de-Teran, H.; Aqvist, J. Linear Interaction Energy: Method and Applications in Drug Design. In *Computational Drug Discovery and Design*; Baron, R., Ed.; Springer: New York, 2012; pp 305−323.

(52) Osterberg, F.; Aqvist, J. Exploring blocker binding to a homology model of the open hERG K+ channel using docking and molecular dynamics methods. *FEBS Lett.* **2005**, *579*, 2939−2944.

(53) Gutierrez-de-Teran, H.; Nervall, M.; Dunn, B. M.; Clemente, J. C.; Aqvist, J. Computational analysis of plasmepsin IV bound to an allophenylnorstatine inhibitor. *FEBS Lett.* **2006**, *580*, 5910−5916.

(54) Ander, M.; Luzhkov, V. B.; Aqvist, J. Ligand binding to the voltage-gated Kv1.5 potassium channel in the open state: Docking and computer simulations of a homology model. *Biophys. J.* **2008**, *94*, 820−831.

(55) Tina, K. G.; Bhadra, R.; Srinivasan, N. PIC: Protein interactions calculator. *Nucleic Acids Res.* **2007**, *35*, 473−476.